2022

A modulated structure derived from the XA-type Mn_2RuSn Heusler compound

Xingzhong Li

Wen-Yong Zhang

Ralph Skomski

David J. Sellmyer

STRUCTURAL SCIENCE CRYSTAL ENGINEERING MATERIALS

ISSN 2052-5206

A modulated structure derived from the XA-type Mn_2RuSn Heusler compound

Xing-Zhong Li,[a]* Wen-Yong Zhang,[b] Ralph Skomski[a,b] and David Sellmyer[a,b]

[a]Nebraska Center for Materials and Nanoscience, University of Nebraska, Lincoln, NE 68588, USA, and [b]Department of Physics, University of Nebraska, Lincoln, NE 68588, USA. *Correspondence e-mail: xzli@unl.edu

Received 20 December 2021
Accepted 24 March 2022

Edited by J. Hadermann, University of Antwerp, Belgium

Keywords: Mn_2RuSn; Heusler compounds; modulated structure; TEM; *Landyne* software.

A modulated structure derived from the inverse Heusler phase (the XA-type and the disordered variant $L2_1B$-type) has been observed in rapidly quenched Mn_2RuSn ribbons. The powder X-ray diffraction pattern of the quenched ribbons can be indexed as an $L2_1B$-type structure. Electron diffraction patterns of the new structure mostly resemble those of the XA-type (and the disordered variant $L2_1B$-type) structure and additional reflections with denser spacing indicate a long periodicity. Orthogonal domains of the modulated structure were revealed by a selected-area electron diffraction pattern and the corresponding dark-field transmission electron microscopy images. The structure was further studied by the crystallographic analysis of high-resolution transmission electron microscopy images. A model for the modulated structure has been proposed to interpret the experimental results.

1. Introduction

Heusler compounds (Felser *et al.*, 2015; Felser & Hirohata, 2016) are a remarkable class of intermetallic materials with wide-ranging and tunable properties. They are in a general composition of XYZ (half-Heusler) or X_2YZ (full-Heusler), where the X and Y atoms are transition metals or lanthanides (rare-earth metals) and the Z atom is always formed by a main group metal or a semimetal. The Heusler compounds include half-metallic ferrimagnetic and ferromagnetic materials, shape memory alloys, high potential magnetocaloric materials, topological insulators and materials for spintronic applications.

The Mn_2RuSn Heusler compound was reported as an $L2_1B$-type cubic phase, a = 0.62195 nm by Endo *et al.* (2012) and Kreiner *et al.* (2014), which is distinguished from the original $L2_1$ structure (or $L2_1A$-type). The $L2_1B$-type structure is a disordered variant of the inverse Heusler structure, XA-type (prototype-$CuHg_2Ti$, space group $F\bar{4}3m$, No. 216), where Mn1 (A) and Mn2 (B) atoms occupy the Wyckoff 4a (0, 0, 0) and 4d ($\frac{3}{4}$, $\frac{3}{4}$, $\frac{3}{4}$) positions, Ru (C) and Sn (D) atoms occupy the 4b ($\frac{1}{2}$, $\frac{1}{2}$, $\frac{1}{2}$) and 4c ($\frac{1}{4}$, $\frac{1}{4}$, $\frac{1}{4}$) positions, respectively. In the $L2_1B$-type structure, the sites at A and C are in a disordered occupation of Mn or Ru.

The site preference, electronic structure and magnetism of the Mn_2RuSn Heusler compound have been investigated using theoretical calculations (Chen *et al.*, 2014; Yang *et al.*, 2015; Shimosakaida & Fujii, 2016). The XA-type structure was confirmed to be the most stable structure in Mn_2RuSn and the moments of the two Mn atoms in the cell are in antiparallel alignment. However, considering the energy difference between the XA-type and $L2_1B$-type structure is relatively

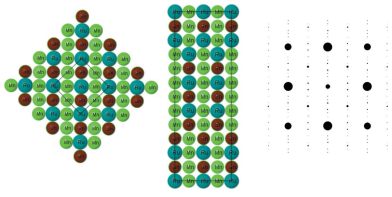

small in Mn_2RuSn, a degree of disorder between Mn (*A*) and Ru (*C*) is likely to occur in agreement with the experimental works mentioned above.

Antiphase boundary (APB), as one of the important micro- or nanostructures, was investigated in the Heusler compounds to explore its effects on magnetic properties, *e.g.* domains, spin-polarization and exchange interactions (Lapworth *et al.*, 1971; Venkateswaran *et al.*, 2007; Umetsu *et al.*, 2011; Murakami *et al.*, 2013; Nedelkoski *et al.*, 2016; Niitsu *et al.*, 2017; Vronka *et al.*, 2020; Levin *et al.*, 2021). Intensive studies on the APB and its related long-periodic structures were initially investigated in AuCu, $AuCu_3$ and Au_3Cu (Ogawa & Watanabe, 1954; Glossop & Pashley, 1959; Yamaguchi *et al.*, 1962; Toth & Sato, 1964; Hashimoto & Ogawa, 1970; Sinclair & Thomas, 1975). The long-periodic structures made from the APBs were also investigated as modulated structures in many alloy systems later on (Miida *et al.*, 1980; Shao, 1999; Linden *et al.*, 2017).

In this paper, we report a new modulated structure derived from the XA-type structure and its orthogonal domains in the Mn_2RuSn Heusler alloy. The structural characterization was carried out using X-ray powder diffraction (XRD), selected-area electron diffraction (SAED), transmission electron microscopy (TEM) dark-field (DF) imaging, and high-resolution transmission electron microscopy (HRTEM) imaging techniques. A structural model of the new structure has been proposed to interpret the experimental results.

2. Materials and methods

An alloy button with a nominal composition of Mn_2RuSn was prepared by arc melting high-purity (99.95%) constituent elements in an argon atmosphere. In order to compensate for Mn loss, an extra 20% Mn and an extra 3% Sn by weight were added during arc melting. The rapidly quenched ribbons were synthesized by ejecting induction-melted solutions of the Mn_2RuSn alloy onto the surface of a copper wheel rotating at a speed of 28 m s^{-1} in a chamber filled with highly pure argon. Then they were annealed in a tubular furnace at a base pressure of 10^{-7} Torr (1 Torr =133.3224 Pa) and temperatures of 900°C for 2 h. These ribbons are about 2 mm wide and 50 µm thick. The ribbon sample was examined using a Malvern PANalytical Empyrean X-ray diffractometer with Cu radiation (λ = 1.5406 Å). The XRD pattern was analyzed with *POWDER CELL* (version 2.4 for *Windows*; Kraus & Nolze, 1996) software.

The ribbon samples were further cut into pieces approximately 2 mm long and mechanically ground and polished to approximately 30 µm or thinner. The samples were then mounted onto 3.05 mm-diameter TEM Cu rings and milled to electron transparency using a Gatan PIPS II under the conditions of an argon ion beam at 4 kV, with an angle starting at 10° and then decreasing to 6°. The TEM experiments were carried out on a Thermo Fisher Scientific Tecnai Osiris microscope equipped with a Gatan Orius CCD camera. The microscope operates at 200 kV and is equipped with a double-tilt TEM holder. The elemental compositions were checked using energy-dispersive X-ray spectroscopy (EDS) and elemental mapping in scanning transmission electron microscopy (STEM) mode. The simulation and analysis of SAED patterns and crystallographic processing of HRTEM images were carried out using the *Landyne* software (Li, 2019, 2021).

3. Results and discussion

The chemical composition of the ribbon samples has been determined by EDS analysis. The average result is Mn 50.2 at.% Ru 25.1 at.% Sn 24.7 at.%, close to the nominal composition of Mn_2RuSn. Fig. 1 shows a STEM high-angle annular dark-field (HAADF) image and EDS maps of Mn, Ru, Sn elements. Besides one bright spot on the boundary of the Mn map and a few spots of color change due to the thinner areas, the ribbon sample shows the homogeneous distribution of Mn, Ru and Sn, which suggests the existence of a single alloy phase with a composition close to Mn_2RuSn.

As mentioned above, the intermetallic phase with a composition of Mn_2RuSn was reported as the inverse Heusler phase (XA-type) with a prototype-$CuHg_2Ti$ or its disordered variant ($L2_1B$). Fig. 2 shows the experimental XRD pattern of the ribbon sample. The peak positions are indexed in the XA-type or $L2_1B$-type structures. The strong (004) peak reveals a (001) texture in the ribbon sample. The XA-type and $L2_1B$-type structures can be further distinguished by comparing the intensity ratio of two diffraction lines, such as $I_{(111)}/I_{(220)}$. The analysis confirms that the sample is of $L2_1B$ type, which is in agreement with reports in the literature (Endo *et al.*, 2012 and Kreiner *et al.*, 2014). In the $L2_1B$-type structure, the Mn atoms and Ru randomly occupy the *A* and *C* sites. The height of the

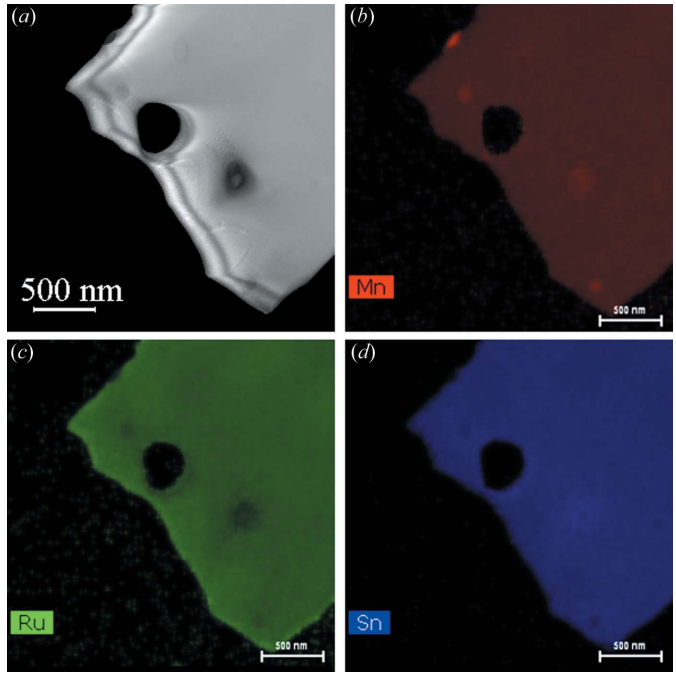

Figure 1
(*a*) A STEM HAADF image and (*b*), (*c*) and (*d*) composition mappings of Mn, Ru and Sn, respectively on the Mn_2RuSn ribbon sample.

(002) peak is related to that the total occupancy of Mn and Ru at the *A* and *C* sites. In the current case, the value is 0.85, less than 1, which means that the *A* and *C* sites are not fully occupied.

Figs. 3(*a*)–3(*c*) show the experimental SAED patterns of the crystal structure in rapidly quenched Mn_2RuSn ribbons and Figs. 3(*d*)–3(*f*) the corresponding ones calculated from the structure of the XA-type Mn_2RuSn phase. The experimental patterns resemble the calculated ones as shown on the distribution of the strong diffraction spots. However, additional reflections with denser spacing can be found in Fig. 3(*a*), which correspond to the extinction positions in Fig. 3(*d*), *e.g.* (110). The two columns of diffraction spots including denser spacing pairs are marked with short vertical bars in Fig. 3(*a*). The observation means that the crystal phase is a new modulated structure derived from the XA-type phase. The indices of the diffraction spots and the zone axes are labeled on the simulated patterns. The simulated SAED patterns were carried out for both the XA-type structure and the disordered variant ($L2_1B$). There are hardly distinguishable for the two sets of the simulated SAED patterns. For example, the simulated SAED patterns of XA and $L2_1B$ along the zone axis [112], we have $I_{(11\bar{1})}/I_{(\bar{2}20)}$ for XA = 10/30 and $I_{(11\bar{1})}/I_{(\bar{2}20)}$ for $L2_1B$ = 9/30. So only the simulated SAED patterns from the XA-type structure are shown here to compare with the experimental SAED patterns.

Similar phenomena on SAED patterns were intensively investigated in the AuCu, $AuCu_3$, and Au_3Cu alloys for the $L1_0$ and $L1_2$ structures and were also reported in the Al–Ti–V alloy for the B2 structure (Shao, 1999). The reflections with denser spacing were interpreted as the formation of long periodic APBs. The reason for reflections with denser spacing in Fig. 3(*a*) may be interpreted in the light of the early works on the AuCu, $AuCu_3$ and Au_3Cu systems.

Fig. 4(*a*) shows an experimental SAED pattern with the selected-area aperture on the grain in the center-left position, which can be viewed as a composite of the one in Fig. 3(*a*) and the same one with 90° rotation. TEM DF images were taken using each pair of reflections with denser spacing with circled marks in Fig. 4(*a*) to reveal the existence of the domains of the new modulated structure. The bright and dark domains in Figs. 4(*b*) and 4(*c*) can be viewed as a pair of jigsaw-like patterns, *i.e.* the bright domain in Fig. 4(*b*) matches the dark

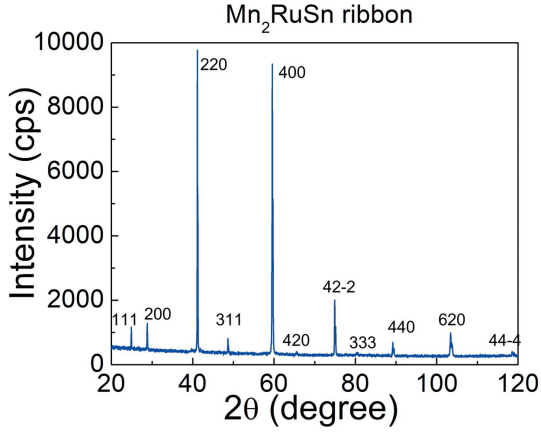

Figure 2
The experimental XRD pattern of the ribbon sample with a composition close to Mn_2RuSn.

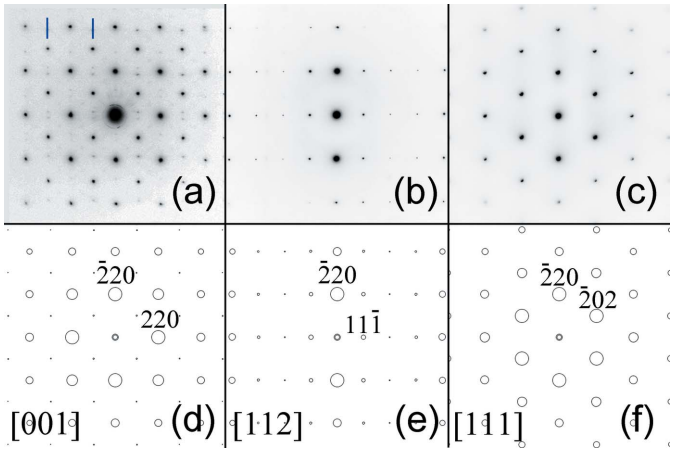

Figure 3
(*a*)–(*c*) Experimental SAED patterns of a new modulated structure derived from the XA-type phase in rapidly quenched Mn_2RuSn ribbons, the simulated SAED patterns along (*d*) [001], (*e*) [112] and (*f*) [111] zone axes were calculated from the XA-type structure.

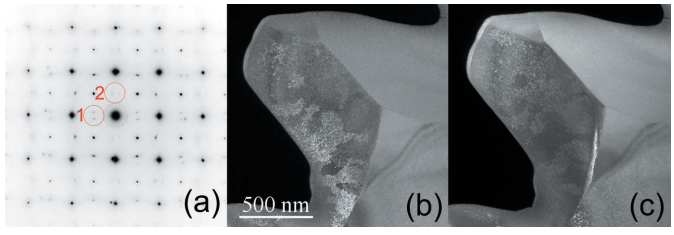

Figure 4
(*a*) A composite SAED pattern of the new modulated structure. Diffraction spot pairs with denser spacing in horizontal and vertical arrays are marked in circles. (*b*, *c*) TEM DF images of the modulated structure, each of them were taken with the spot pair marked in circles in (*a*).

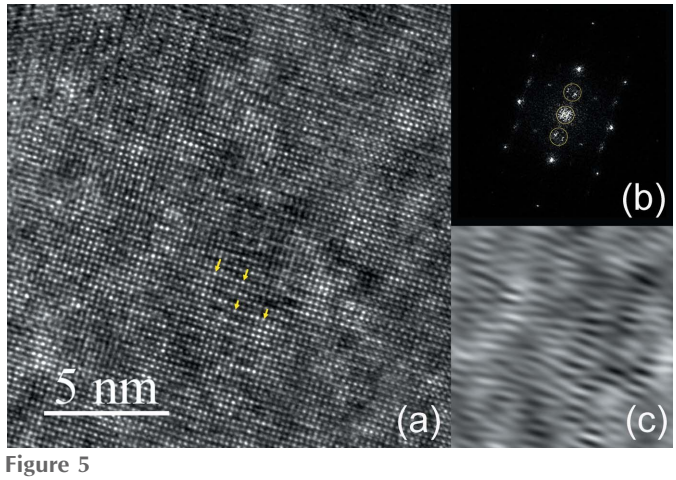

Figure 5
(*a*) An HRTEM image of the Mn_2RuSn ribbons along the [001] zone axis, (*b*) an FFT pattern of the HRTEM image, (*c*) an inverse FFT image with a filter to select the nearest diffraction spot pairs with denser spacing and central spot. The filter is shown in Fig. 4(*b*) as three open circles.

domain in Fig. 4(*c*) and *vice versa*. The size of the domains was estimated in the range of 100 nm to 300 nm.

Fig. 5(*a*) shows the HRTEM image taken from the Mn_2RuSn ribbon samples along the [001] zone axis, Fig. 5(*b*) an FFT pattern of the central area of the image and Fig. 5(*c*) an inverse FFT image with a filter to select the two nearest diffraction spot pairs with denser spacing and central spot. The filter is shown in Fig. 5(*b*) as three circles. Fig. 5(*c*) can be viewed as a higher magnification version of the DF images in Figs. 4(*b*) and 4(*c*). As analyzed above, the TEM DF images cover two orientations of the antiphase domains. In contrast, the HRTEM image was taken within an area with only one orientation of the antiphase domain. Fig. 5(*c*) shows dark and bright segments with a length of six image spots on average. Two strings of continuous brighter six image spots are marked in Fig. 5(*a*) as examples. This analysis also gives us a clue to build a structural model using the XA-type structure with periodic stacking of the APBs and then to adjust the atom occupancy according to the $L2_1$B-type structure.

As we know, two types of APB were reported in the Heusler alloys: a $\frac{a}{4}$[111] shift APB in the half-metallic Heusler alloy $Co_2Fe(Al,Si)$ (Niitsu *et al.*, 2017) and a $\frac{a}{2}$[100] shift APB in the Heusler alloy $Ni_{50}Mn_{20}In_{30}$ (Vronka *et al.*, 2020). We found that the second type of APB should be in the Heusler alloy Mn_2RuSn and it was adopted to build the structural model as below. Fig. 6(*a*) shows the lattice of the Mn_2RuSn XA-type structure projection viewed in the **c** direction. A 45°-tilted unit cell is outlined with dashed lines and labeled A, $b = a$. The same unit cell with a $\frac{a}{2}$[100] shift from *A* is labeled *B*. The basic modulated structures with APB can be constructed in a sequence of *ABAB* in Fig. 6(*b*), the unit-cell parameters are $a' = a$ and $b' = 2a$; in a sequence of *AABAAB* in Fig. 6(*c*),

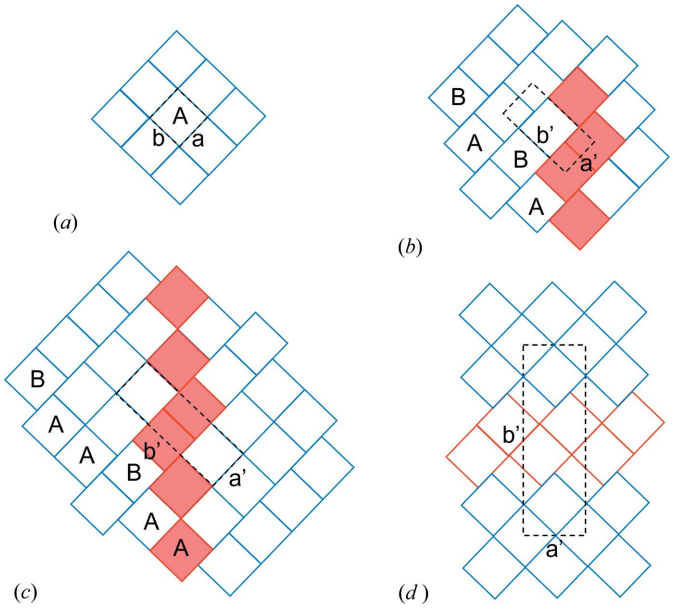

Figure 6
A schematical drawing of (*a*) the XA structure, (*b*) a modulated structure of *AB* packing with APB, (*c*) a modulated structure of *AAB* packing with APB, and (*d*) the model for the new modulated structure. The local arrangement configure in (*d*) is similar to those in (*b*) and (*c*).

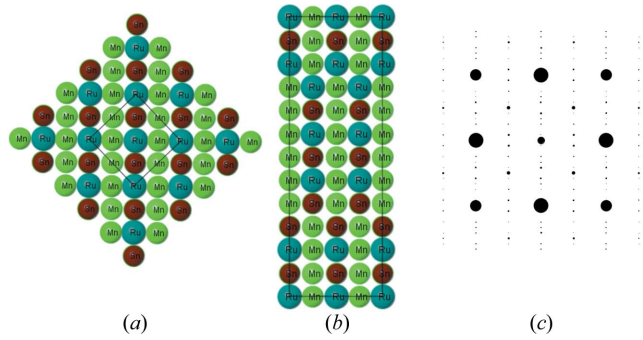

Figure 7
(*a*) Projection of the Mn_2RuSn XA-type structure. (*b*) Structural projection of the modulated model. (*c*) The simulated SAED patterns of the model along the [001] zone axis.

the unit-cell parameters are $a' = a$ and $b' = 3a$. However, the simulated SAED patterns on the basis of the two simple models do not agree with the experimental SAED pattern in Fig. 3(*a*). On account of the HRTEM image analysis above, we proposed a modulated structure with the building bocks and lattice in Fig. 6(*d*), the unit-cell parameters, $a' = \sqrt{2}a$ and $b' = 3\sqrt{2}a$. The modulated structure can be viewed as two blocks of XA unit cells, one with three unit cells in a row and the other with two unit cells in a row, separated with the $\frac{a}{2}$[100] shift APBs. The local arrangement configuration in Fig. 6(*d*) is similar to those in Figs. 6(*b*) and 6(*c*), as marked in gray shadow (red color in the online version).

The projections of the XA structure and the modulated model are shown in Figs. 7(*a*) and 7(*b*) for comparison. The atom distribution near APBs in the modulated model is adjusted locally to make lines of six Mn atoms or lines of three Ru and three Sn atoms in Fig. 7(*b*). The XA-type structure can be viewed as four different atom layers along the [001] direction. The layers 1 and 3 consist of the atoms Mn (*A* site) and Ru (*C* site), the layers 2 and 4 consist of the atoms Mn (*B* site) and Sn (*D* site). In the $L2_1$B-type structure, layers 1 and 3 are chemical-disordered atom layers. In the present model, we assume that only one of layers (1 or 3) is in a disordered state. The disorder order layer is not shown in Fig. 7(*b*). Simulation of the SAED patterns based on the model in three variations were carried out, (i) only one of the layers (1 or 3) is in a disordered state, (ii) both layers (1 and 3) are in a disordered state, and (iii) both layers (1 and 3) are in an ordered state. Fig. 7(*c*) shows the simulated SAED pattern based on the first variation, *i.e.* only one of the layers (1 or 3) is in a disordered state, which is the best one to match the main features of the experimental SAED pattern in Fig. 3(*a*). The model can be considered an ideal structure compared to the actual nanostructure, as revealed by the HRTEM image in Fig. 5.

4. Concluding remarks

In summary, a new modulated structure of the XA-type phase has been observed in rapidly quenched Mn_2RuSn ribbons. Orthogonal domains of the modulated structure were revealed by the SAED pattern along the [001] zone axis and

corresponding TEM DF images. A structural model has been proposed to interpret the experimental results.

Acknowledgements

The work was performed in part in the Nebraska Nanoscale Facility, National Nanotechnology Coordinated Infrastructure, and the Nebraska Center for Materials and Nanoscience, supported by the National Science Foundation under Award ECCS: 2025298 and the Nebraska Research Initiative.

Funding information

The following funding is acknowledged: National Science FoundationD, Designing Materials to revolutionize and engineer our future (grant No. 1729288).

References

Chen, J.-G., Luo, H.-Z., Jia, P.-Z., Meng, F.-B., Liu, G.-D., Liu, E.-K., Wang, W.-H. & Wu, G.-H. (2014). *J. Magn. Magn. Mater.* **365**, 132–137.

Endo, K., Kanomata, T., Nishihara, H. & Ziebeck, K. R. A. (2012). *J. Alloys Compd.* **510**, 1–5.

Felser, C. & Hirohata, A. (2016). *Heusler Alloys. Properties, Growth, Applications.* Springer International Publishing Switzerland.

Felser, C., Wollmann, L., Chadov, S., Fecher, G. H. & Parkin, S. S. P. (2015). *APL Mater.* **3**, 041518.

Glossop, A. B. & Pashley, D. W. (1959). *Proc. R. Soc. London. Ser. A, Math. Phys. Sci.* **250**, 132–146.

Hashimoto, S. & Ogawa, S. (1970). *J. Phys. Soc. Jpn*, **29**, 710–721.

Kraus, W. & Nolze, G. (1996). *J. Appl. Cryst.* **29**, 301–303.

Kreiner, G., Kalache, A., Hausdorf, S., Alijani, V., Qian, J.-F., Shan, G.-C., Burkhardt, U., Ouardi, S. & Felser, C. (2014). *Z. Anorg. Allg. Chem.* **640**, 738–752.

Lapworth, A. J., Jakubovics, J. P. & Baker, G. S. (1971). *J. Phys. Colloq.* **32**, C1-259–C1-260.

Levin, E. E., Kitchaev, D. A., Eggeler, Y. M., Mayer, J. A., Behera, P., Gianola, D. S., Van der Ven, A., Pollock, T. M. & Seshadri, R. (2021). *Phys. Rev. Mater.* **5**, 014408.

Li, X.-Z. (2019). *Microscopy and Analysis*, May issue, pp. 16–19. Wiley Analytical Science. https://analyticalscience.wiley.com/do/10.1002/micro.2877.

Li, X.-Z. (2021). *SIMPA*, structural image processing and analysis, *Microscopy and Microanalysis* (in preparation); also, in https://landyne.com.

Linden, Y., Pinkas, M., Munitz, A. & Meshi, L. (2017). *Scr. Mater.* **139**, 49–52.

Miida, R., Kasahara, M. & Watanabe, D. (1980). *Jpn. J. Appl. Phys.* **19**, L707–L710.

Murakami, Y., Yanagisawa, K., Niitsu, K., Park, H. S., Matsuda, T., Kainuma, R., Shindo, D. & Tonomura, A. (2013). *Acta Mater.* **61**, 2095–2101.

Nedelkoski, Z., Sanchez, A. M., Ghasemi, A., Hamaya, K., Evans, R. F. L., Bell, G. R., Hirohata, A. & Lazarov, V. K. (2016). *Appl. Phys. Lett.* **109**, 222405.

Niitsu, K., Minakuchi, K., Xu, X., Nagasako, M., Ohnuma, I., Tanigaki, T., Murakami, Y., Shindo, D. & Kainuma, R. (2017). *Acta Mater.* **122**, 166–177.

Ogawa, S. & Watanabe, D. (1954). *J. Phys. Soc. Jpn*, **9**, 475–488.

Shao, G. S. (1999). *Appl. Phys. Lett.* **74**, 2643–2645.

Shimosakaida, K. & Fujii, S. (2016). *Mater. Trans.* **57**, 312–315.

Sinclair, R. & Thomas, G. (1975). *J. Appl. Cryst.* **8**, 206–210.

Toth, R. S. & Sato, H. (1964). *J. Appl. Phys.* **35**, 698–703.

Umetsu, R. Y., Ishikawa, H., Kobayashi, K., Fujita, A., Ishida, K. & Kainuma, R. (2011). *Scr. Mater.* **65**, 41–44.

Venkateswaran, S. P., Nuhfer, N. T. & De Graef, M. (2007). *Acta Mater.* **55**, 2621–2636.

Vronka, M., Straka, L., De Graef, M. & Heczko, O. (2020). *Acta Mater.* **184**, 179–186.

Yamaguchi, S., Watanabe, D. & Ogawa, S. (1962). *J. Phys. Soc. Jpn*, **17**, 1030–1041.

Yang, L., Liu, B.-H., Luo, H.-Z., Meng, F.-B., Liu, H.-Y., Liu, E.-K., Wang, W.-H. & Wu, G.-H. (2015). *J. Magn. Magn. Mater.* **382**, 247–251.